Density-functional theory of spherical electric double layers and ζ potentials of colloidal particles in restricted-primitive-model electrolyte solutions

Yang-Xin Yu[a)]
Department of Chemical Engineering, Tsinghua University, Beijing 100084, China

Jianzhong Wu
Department of Chemical and Environmental Engineering, University of California, Riverside, California 92521-0425

Guang-Hua Gao
Department of Chemical Engineering, Tsinghua University, Beijing 100084, China

(Received 1 December 2003; accepted 21 January 2004)

A density-functional theory is proposed to describe the density profiles of small ions around an isolated colloidal particle in the framework of the restricted primitive model where the small ions have uniform size and the solvent is represented by a dielectric continuum. The excess Helmholtz energy functional is derived from a modified fundamental measure theory for the hard-sphere repulsion and a quadratic functional Taylor expansion for the electrostatic interactions. The theoretical predictions are in good agreement with the results from Monte Carlo simulations and from previous investigations using integral-equation theory for the ionic density profiles and the ζ potentials of spherical particles at a variety of solution conditions. Like the integral-equation approaches, the density-functional theory is able to capture the oscillatory density profiles of small ions and the charge inversion (overcharging) phenomena for particles with elevated charge density. In particular, our density-functional theory predicts the formation of a second counterion layer near the surface of highly charged spherical particle. Conversely, the nonlinear Poisson–Boltzmann theory and its variations are unable to represent the oscillatory behavior of small ion distributions and charge inversion. Finally, our density-functional theory predicts charge inversion even in a 1:1 electrolyte solution as long as the salt concentration is sufficiently high. [DOI: 10.1063/1.1676121]

I. INTRODUCTION

When a charged colloidal particle is immersed in an electrolyte solution, it is surrounded by counterions—i.e., small ions of opposite sign—to balance the surface charge. The charged colloidal surface along with the neutralizing diffuse layer of counterions is often referred to as the electric double layer (EDL), which plays an important role in many aspects of interfacial phenomena.[1–3] For instance, the stability of a charge-stabilized colloidal dispersion crucially depends on the distribution of small ions in the EDL.[2] Most electrochemical reactions at interfaces occur within the EDL and the kinetics of these reactions is closely related to small ion distributions.[4] Besides, the structure of an EDL provides the microscopic details for a rational explanation and prediction of the electrostatic mobility of charged colloidal particles including globular proteins.[5,6]

An EDL may be planar,[4,7–18] cylindrical,[5,19–22] spherical,[3,23–26] or ellipsoidal[27] depending on the geometry of the charged surface. In the past two decades, the planar EDL has been extensively investigated using computer simulations,[7,11,17] integral-equation (IE) theories,[8,13,16] and density-functional theories (DFTs).[9,10,12,14–16] There are many excellent reviews on the theoretical description of planar EDLs (see, for example, Ref. 18). However, relatively fewer studies have been reported on EDLs of other geometries. In this work, we are concerned with spherical EDLs in particular because many practical applications of colloid systems, such as inorganic sols, soap solutions, and aqueous solutions of globular proteins, are mainly involved with spherical macropaticles. The planar EDL can be regarded as a special case of the spherical EDL when the radius approaches infinity.

The conventional theory for describing the ionic distributions and the mean electrostatic potential in the spherical EDL is provided by the Poisson–Boltzmann (PB) equation.[26] In this mean-field approach, the colloidal particles are taken to be hard spheres of radius R with a uniform surface charge density Q, and the ionic solution is represented by point charges immersed in a dielectric continuum. The distributions of small ions and subsequent thermodynamic properties are calculated from a numerical solution of the PB equation.[28] For colloids of finite concentrations, the Wigner–Seitz cell model[29] has been proposed to represent the overlapping EDLs of neighboring colloidal particles. While theoretical approaches based on the PB equation have been successful in representing a variety of electrostatic phenomena, they are often inadequate for highly charged systems

[a)]Corresponding author. Electronic mail: yangxyu@mail.tsinghua.edu.cn

where the correlations between small ion distributions are significant.[30,31] Ionic correlations may lead to new phenomena in colloidal dispersions that contradict predictions from the Poisson–Boltzmann equation (and its variations). A well-known example is charge inversion, or overcharging, of colloidal particles of high surface charge density. In this case, counterions are accumulated close to the colloidal surface such that the overall charge has opposite sign of the bare charge.[32,33] Charge inversion is a broad phenomenon and there may be a host of physical scenarios which can lead to macroion overcharging.[34] This has been observed by Strauss *et al.*[35] in their experimental work on the electrophoretic mobility of a polysoap and was confirmed later by both computer simulations[36] and liquid-state theories.[8]

The importance of correlations between the small ions on the structure of spherical EDLs has been well addressed by IEs (Refs. 8 and 37) and the fifth-order modification of the PB equation (MPB5).[23,38] In these more sophisticated theories, the ionic solution is often represented by a so-called restricted primitive model (RPM) where the small ions are charged particles of uniform size and the solvent is a continuous dielectric medium. One popular approach is represented by the hypernetted chain (HNC) closure to the Ornstein–Zernike (02) equation.[8,39] Specifically, two versions of the HNC equations have been proposed to study EDLs. In both versions, the HNC closure is applied to representing the correlations between macroparticles and small ions. For the correlations among small ions, one also relies on the HNC closure, whereas the other applies analytical expressions from the mean-spherical approximation (MSA). We refer to the former as the HNC/HNC (Ref. 37) theory and the latter as the HNC/MSA theory.[3,8] Although the HNC/HNC theory appears theoretically more consistent, the HNC/MSA theory is numerically much more convenient and accurate, especially for colloids in electrolyte solutions of low concentration.[3] The HNC/MSA theory has been successfully used in the calculation of ζ potentials in electrophoresis experiments.[6,40]

Both IE and MPB5 studies indicated that, whereas the PB equation is sufficient for monovalent electrolyte solutions at relatively low concentrations (less than 0.1 mol), the correlations between small ions become important for multivalent salts and for electrolyte solutions of higher concentrations. Particularly, the HNC/MSA theory and MPB5 predict a maximum ζ potential of macroparticles as a function of surface charge density, in contrast to the prediction of the original PB theory.

Density-functional theory represents a powerful alternative to the PB equation and IE theories.[41–43] In a typical DFT approach for describing EDLs, the excess Helmholtz energy due to the hard-sphere repulsion is given by a weight-density approximation (e.g., Tarazona recipe[41]) and that due to the electrostatic interactions is taken into account by a quadratic expansion of the excess Helmholtz energy functional with respect to that for a uniform fluid. The DFT with the MSA bulk direct correlation function as the input has already been applied to the planar EDL.[9,10,12,14,16] To improve the performance of DFT for ions that are strongly coupled, Boda *et al.*[15] used the generalized MSA (GMSA) (Ref. 44) to describe the bulk fluid. This improvement can account for the drying phenomena of the planar electrode. Using DFT, Patra and Yethiraj[19,22] investigated the ionic density profiles, mean electrostatic potentials, and preferential interaction coefficients for the cylindrical EDL with the axial charge densities corresponding to DNA. To our best knowledge, DFT has not been applied to the spherical EDL so far. Various DFTs for the structures of EDLs have been recently reviewed by Hansen and Lowen.[30] Previous applications of DFT for the planar and cylindrical EDLs indicate that for colloidal particles dispersed in electrolyte solutions of monovalent ions, DFT, PB, and HNC/HNC theories yield comparable results. However, DFT is more accurate than other approaches in the presence of multivalent ions or in mixed electrolyte solutions.[10,16,19]

Charge inversion can be explained by both IE theories and DFTs quantitatively.[6,20,45–49] Previous investigations suggested that charge inversion occurs only in solutions containing multivalent counterions.[6,20,46–48] Using molecular dynamics simulations and an IE theory, Messina *et al.*[32] studied the effect of an excluded volume of small ions on charge inversion in great detail. They also observed charge inversion with monovalent ion systems in a double layer. Recent advances in the physics of charge inversion in chemical and biological systems have been reviewed by Grosberg *et al.*[50] and Levin.[31]

In this work, we present a partially perturbative DFT for an isolated charged macroparticle immersed in restrictive-primitive-model electrolyte solutions. The excess free-energy functional due to hard-sphere repulsion is evaluated through an improved fundamental measure theory[51,52] and the electrical contribution is calculated using a quadratic expansion of the Helmholtz energy functional with respect to that for a uniform fluid of the same chemical potentials. The DFT is applied to investigating the effect of macroparticle radius and charge density, ionic valence, and concentration on the ionic density profiles and to calculating the mean electrostatic potential, ζ potential, and charge inversion of highly charged colloidal particles. We compare the results from DFT with those from Monte Carlo simulations and from previous investigations based on the HNC/MSA integral equation theory and the nonlinear PB equation. Because the structure of EDLs is sensitive to the ionic valence, we consider both symmetrical and asymmetrical electrolytes.

The rest of this paper is organized as the following. Section II describes the DFT theory for spherical EDLs; numerical results for the ionic density profiles, mean electrostatic potentials, ζ potentials, and charge inversions are presented in Sec. III. Finally, Sec. IV concludes with a few general remarks and perspectives for future work.

II. THEORY

A. Model

We consider an isolated spherical particle dispersed in an aqueous electrolyte solution within the restrictive primitive model.[39] The macroparticle is a charged hard sphere with a surface charge density Q given by

$$Q=\frac{Ze}{4\pi R^2}, \tag{1}$$

where e is the electron charge, and Z and R are, respectively, the valence and radius of the macroparticle. The small ions are taken to be charged hard spheres of equal diameter σ and the solvent is represented by a continuous dielectric medium. The dielectric constant of the solvent is $\varepsilon=78.5$, corresponding to that for water at $T=298$ K. The pair potential between ions i and j is given by

$$u_{ij}(r)=\begin{cases}\infty, & r<\sigma,\\ \dfrac{z_i z_j e^2}{\varepsilon r}, & r\geqslant\sigma,\end{cases} \tag{2}$$

where z_i is the valence of ion i and r is the center-to-center distance. The unscreened macroparticle–ion potential $V_{Mj}(r)$ is similarly given by

$$V_{Mj}(r)=\begin{cases}\infty, & r<R+\sigma/2\\ \dfrac{4\pi R^2 Q z_j e}{\varepsilon r}, & r\geqslant R+\sigma/2.\end{cases} \tag{3}$$

Throughout this work, if not pointed out, the temperature T is set to be 298 K and the diameter of small ions is 0.425 nm.

B. Density-functional theory

The grand potential for small ions surrounding an isolated charged macroparticle is related to the Helmholtz energy functional for the small ions through the Legendre transform

$$\Omega[\{\rho_i\}]=F[\{\rho_i\}]+\sum_{i=1}^{N}\int d\mathbf{r}[V_{Mi}(\mathbf{r})-\mu_i]\rho_i(\mathbf{r}), \tag{4}$$

where $\{\rho_i\}$ is a set of density distributions for all small ions, N is the total number of ionic species, μ_i is the chemical potential of ion i, and $F[\{\rho_i\}]$ represents the Helmholtz energy functional.

The essential task of a density-functional theory is to derive an analytical expression for the Helmholtz free energy F as a functional of the density distributions. Without loss of generality, we may decompose F into four parts—i.e.,

$$F[\{\rho_i\}]=F^{\mathrm{id}}[\{\rho_i\}]+F_{\mathrm{hs}}^{\mathrm{ex}}[\{\rho_i\}]+F_{\mathrm{C}}^{\mathrm{ex}}[\{\rho_i\}]+F_{\mathrm{el}}^{\mathrm{ex}}[\{\rho_i\}], \tag{5}$$

where $F^{\mathrm{id}}[\{\rho_i\}]$ is the ideal-gas contribution, $F_{\mathrm{hs}}^{\mathrm{ex}}[\{\rho_i\}]$ is the hard-sphere contribution, $F_{\mathrm{C}}^{\mathrm{ex}}[\{\rho_i\}]$ is the direct Coulomb contribution, and $F_{\mathrm{el}}^{\mathrm{ex}}[\{\rho_i\}]$ represents a coupling of Coulombic and hard-sphere interactions. The ideal-gas contribution is given by the exact expression

$$F^{\mathrm{id}}[\{\rho_i\}]=k_BT\sum_{i=1}^{N}\int d\mathbf{r}\,\rho_i(\mathbf{r})[\ln(\rho_i(\mathbf{r})\lambda_i^3)-1], \tag{6}$$

where $\lambda_i=(h^2/2\pi m_i k_B T)^{1/2}$ is the thermal de Broglie wavelength of component i and k_B is the Boltzmann constant. The direct Coulomb contribution is also known exactly, given by

$$F_{\mathrm{C}}^{\mathrm{ex}}[\{\rho_i\}]=\frac{1}{2}\int\int d\mathbf{r}_1 d\mathbf{r}_2\sum_{i,j}\frac{z_i z_j e^2\rho_i(\mathbf{r}_1)\rho_j(\mathbf{r}_2)}{\varepsilon|\mathbf{r}_1-\mathbf{r}_2|}. \tag{7}$$

To find expressions for $F_{\mathrm{hs}}^{\mathrm{ex}}[\{\rho_i\}]$ and $F_{\mathrm{el}}^{\mathrm{ex}}[\{\rho_i\}]$ (both are ignored in the nonlinear PB equation), we use a modified fundamental measure theory (MFMT) developed recently[51] and a quadratic expansion of the Helmholtz energy functional.[12] According to MFMT, $F_{\mathrm{hs}}^{\mathrm{ex}}[\{\rho_i\}]$ is given by

$$\beta F_{\mathrm{hs}}^{\mathrm{ex}}=\int\Phi^{\mathrm{hs}}[n_\alpha(\mathbf{r})]d\mathbf{r}, \tag{8}$$

where $\Phi^{\mathrm{hs}}[n_\alpha(\mathbf{r})]$ is the reduced excess Helmholtz energy density due to hard-sphere repulsion, $\beta=1/k_BT$, and $n_\alpha(\mathbf{r})$ is the weighted density. As in Rosenfeld's original FMT,[53] the weighted densities are defined as

$$n_\alpha(\mathbf{r})=\sum_{i=1}^{N}n_{\alpha i}(\mathbf{r})=\sum_{i=1}^{N}\int\rho_i(\mathbf{r}')w_i^{(\alpha)}(|\mathbf{r}'-\mathbf{r}|)d\mathbf{r}', \tag{9}$$

where the subscripts $\alpha=0$, 1, 2, 3, $V1$, and $V2$ denote the index of six weight functions $w_i^{(\alpha)}(\mathbf{r})$ that characterize the volume, surface area, and surface vector averages of a spherical particle i.

The six weight functions are independent of the density profiles. Among them, three weight functions are directly related to the geometry of a spherical particle i:

$$w_i^{(2)}(r)=\delta(\sigma_i/2-r), \tag{10}$$

$$w_i^{(3)}(r)=\theta(\sigma_i/2-r), \tag{11}$$

$$\mathbf{w}_i^{(V2)}(\mathbf{r})=(\mathbf{r}/r)\,\delta(\sigma_i/2-r), \tag{12}$$

where $\delta(r)$ is the Dirac delta function and $\theta(r)$ is the Heaviside step function. Integration of two scalar weight functions $w_i^{(2)}(r)$ and $w_i^{(3)}(r)$ with respect to the position gives the particle surface area and volume, respectively, and integration of the vector weight function $\mathbf{w}_i^{(V2)}(\mathbf{r})$ is related to the gradient across the sphere in the $\mathbf{r}$ direction. Other weight functions are proportional to the three functions given in Eqs. (10)–(12)—i.e.,

$$w_i^{(0)}(r)=\frac{w_i^{(1)}(r)}{\sigma_i/2}=\frac{w_i^{(2)}(r)}{\pi\sigma_i^2} \tag{13}$$

and

$$\mathbf{w}_i^{(V1)}(\mathbf{r})=\frac{\mathbf{w}_i^{(V2)}(\mathbf{r})}{2\pi\sigma_i}. \tag{14}$$

As in our previous work,[51] the hard-sphere Helmholtz energy density consists of contributions from the scalar-weighted densities and the vector-weighted densities:

$$\Phi^{\mathrm{hs}}[n_\alpha(\mathbf{r})]=\Phi^{\mathrm{hs(S)}}[n_\alpha(\mathbf{r})]+\Phi^{\mathrm{hs(V)}}[n_\alpha(\mathbf{r})], \tag{15}$$

where the superscripts (S) and (V) stand for contributions from scalar and vector weighted densities, respectively. The scalar Helmholtz energy density is given by

$$\Phi^{\mathrm{hs(S)}}[n_\alpha(\mathbf{r})]=-n_0\ln(1-n_3)+\frac{n_1n_2}{1-n_3}+\frac{n_2^3\ln(1-n_3)}{36\pi n_3^2}+\frac{n_2^3}{36\pi n_3(1-n_3)^2}, \tag{16}$$

and the vector Helmholtz energy density is given by

$$\Phi^{\mathrm{hs(V)}}[n_\alpha(\mathbf{r})]=-\frac{\mathbf{n}_{V1}\cdot\mathbf{n}_{V2}}{1-n_3}-\frac{n_2\mathbf{n}_{V2}\cdot\mathbf{n}_{V2}}{12\pi n_3^2}\ln(1-n_3)-\frac{n_2\mathbf{n}_{V2}\cdot\mathbf{n}_{V2}}{12\pi n_3(1-n_3)^2}. \tag{17}$$

In the limit of a bulk fluid, the two vector weighted densities $\mathbf{n}_{V1}$ and $\mathbf{n}_{V2}$ vanish, and the Helmholtz free energy density Φ^{hs} becomes identical to that from the Boublik–Mansoori–Carnahan–Starling–Leland (BMCSL) equation of state.[54]

Following the previous work on the DFT of a planar electrical double layer,[41] we make a functional Taylor expansion of the residual Helmholtz free-energy functional around that for a uniform fluid to obtain $F_{\mathrm{el}}^{\mathrm{ex}}[\{\rho_i\}]$:

$$F_{\mathrm{el}}^{\mathrm{ex}}[\{\rho_i\}]=F_{\mathrm{el}}^{\mathrm{ex}}[\{\rho_i^b\}]+\int d\mathbf{r}\sum_{i=1}^{N}\frac{\delta F_{\mathrm{el}}^{\mathrm{ex}}}{\delta\rho_i(\mathbf{r})}[\rho_i(\mathbf{r})-\rho_i^b]+\frac{1}{2}\int\int d\mathbf{r}\,d\mathbf{r}'\sum_{j=1}^{N}\sum_{i=1}^{N}\frac{\delta^2F_{\mathrm{el}}^{\mathrm{ex}}}{\delta\rho_i(\mathbf{r})\,\delta\rho_j(\mathbf{r}')}[\rho_i(\mathbf{r})-\rho_i^b][\rho_j(\mathbf{r}')-\rho_j^b]+\cdots, \tag{18}$$

where $\{\rho_i^b\}$ is the set of all bulk densities. The direct correlation functions due to the residual electrostatic are defined as

$$\Delta C_i^{(1)\mathrm{el}}=-\beta\delta F_{\mathrm{el}}^{\mathrm{ex}}/\delta\rho_i(\mathbf{r}), \tag{19}$$

$$\Delta C_{ij}^{(2)\mathrm{el}}(|\mathbf{r}'-\mathbf{r}|)=-\beta\delta^2F_{\mathrm{el}}^{\mathrm{ex}}/\delta\rho_i(\mathbf{r})\,\delta\rho_j(\mathbf{r}'). \tag{20}$$

If we neglect all higher-order terms $\Delta C_{ijk}^{(n)\mathrm{el}}(n>2)$ in Eq. (18), $F_{\mathrm{el}}^{\mathrm{ex}}[\{\rho_i\}]$ becomes

$$\beta F_{\mathrm{el}}^{\mathrm{ex}}[\{\rho_i\}]=\beta F_{\mathrm{el}}^{\mathrm{ex}}[\{\rho_i^b\}]-\int d\mathbf{r}\sum_{i=1}^{N}\Delta C_i^{(1)\mathrm{el}}[\rho_i(\mathbf{r})-\rho_i^b]-\frac{1}{2}\int\int d\mathbf{r}\,d\mathbf{r}'\sum_{i=1}^{N}\sum_{j=1}^{N}\Delta C_{ij}^{(2)\mathrm{el}}(|\mathbf{r}'-\mathbf{r}|)\times[\rho_i(\mathbf{r})-\rho_i^b][\rho_j(\mathbf{r}')-\rho_j^b]. \tag{21}$$

As the grand potential $\Omega[\{\rho_i\}]$ reaches a minimum at equilibrium, we can derive the Euler–Lagrange equations for the density profiles of small ions:

$$-k_BT\ln[\rho_i(\mathbf{r})/\rho_i^b]=\left[\frac{\delta F_{\mathrm{hs}}^{\mathrm{ex}}}{\delta\rho_i(\mathbf{r})}-\mu_{i,\mathrm{hs}}^{\mathrm{ex}}\right]+z_ie[\psi(\mathbf{r})-\psi^b]-k_BT\sum_{j=1}^{N}\int d\mathbf{r}'\,\Delta C_{ij}^{(2)\mathrm{el}}(|\mathbf{r}'-\mathbf{r}|)\times[\rho_j(\mathbf{r}')-\rho_j^b], \tag{22}$$

where $F_{\mathrm{hs}}^{\mathrm{ex}}$ is evaluated from Eq. (8) and $\psi(\mathbf{r})$ is the mean electrostatic potential that satisfies Poisson's equation. For a spherical electric double layer, the mean electrostatic potential as a function of distance to the center of the macroparticle, $\psi(r)$, can be expressed in terms of the ionic density profiles:

$$\psi(r)=\frac{4\pi e}{\varepsilon}\int_r^\infty\sum_{i=1}^{N}\rho_i(r')z_i\left[r'-\frac{r'^2}{r}\right]dr'. \tag{23}$$

The excess direct correlation function $\Delta C_{ij}^{(2)\mathrm{el}}(r)$ is defined as

$$\Delta C_{ij}^{(2)\mathrm{el}}(r)=C_{ij}(r)+\frac{\beta z_iz_je^2}{\varepsilon r}-C_{ij}^{\mathrm{hs}}(r). \tag{24}$$

$\Delta C_{ij}^{(2)\mathrm{el}}(r)$ can be obtained from, for example, numerical solutions of HNC or hybridized MSA (Ref. 55) closure of the OZ equation. The most popular approach is to calculate $\Delta C_{ij}^{(2)\mathrm{el}}(r)$ from the MSA (which yields analytical expressions in reasonable accuracy). In the restrictive primitive model, the MSA gives $\Delta C_{ij}^{(2)\mathrm{el}}(r)$ (Ref. 56)

$$\Delta C_{ij}^{(2)\mathrm{el}}(r)=\begin{cases}-\dfrac{z_iz_je^2\beta}{\varepsilon}\left[\dfrac{2B}{\sigma}-\left(\dfrac{B}{\sigma}\right)^2r-\dfrac{1}{r}\right], & r<\sigma,\\ 0, & r>\sigma,\end{cases} \tag{25}$$

where

$$B=\Gamma\sigma/(1+\Gamma\sigma) \tag{26}$$

and Γ is related to the inverse of the Debye screening length

$$\kappa^2=(4\pi\beta e^2/\varepsilon)\sum_{i=1}^{N}\rho_i^bz_i^2 \tag{27}$$

by

$$\kappa=2\Gamma(1+\Gamma\sigma). \tag{28}$$

By taking the common small ion radius σ tending to zero, both hard-sphere contributions and interionic correlations in Eq. (22) are eliminated, and if we let $\psi^b=0$, the following expression is obtained:

$$\rho_i(r)/\rho_i^b=\exp[-\beta z_ie\psi(r)]. \tag{29}$$

Obviously, Eq. (29) is the integral version of the nonlinear PB equation for the spherical EDL with the Stern correlation,[3] which does not include the interionic correlations.

Equations (22) and (29) are solved using the standard Picard iterative techniques or a finite-element method.[9] Once the ionic density profiles are known, the charge density on the surface of the macroparticle, Q, is calculated from

$$Q=-\frac{e}{R^2}\int_{R+\sigma/2}^{\infty}\sum_{i=1}^{N}\rho_i(r)z_ir^2dr. \tag{30}$$

III. RESULTS AND DISCUSSION

A. Ionic density profiles

We first discuss the ionic density profiles near a charged macroparticle immersed in symmetrical (1:1 and 2:2) and asymmetrical (1:2 and 2:1) electrolyte solutions at various concentrations and surface charge densities of the macroparticle. To test the performance of the DFT equations and the numerical method, we first consider two limiting cases. One is that the macroion has the same size and charge as one of the small ions of the electrolyte; the other is that the macro-

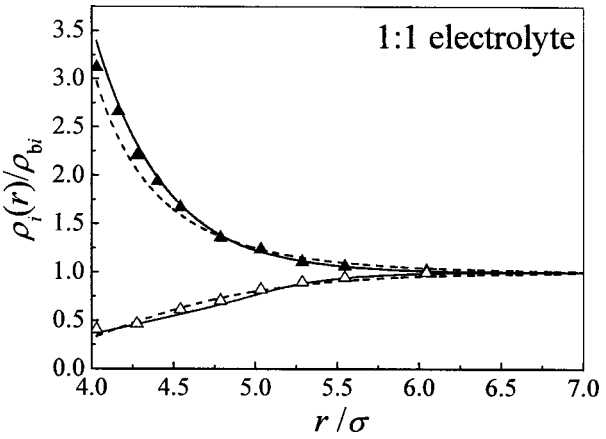

FIG. 1. Density profiles of counterions and coions around a charged spherical macroparticle of radius $R=1.5$ nm and surface charge density $Q=0.102$ C/m^2 dispersed in a 1:1 electrolyte at the bulk concentration $C=1.0$ mol/L. The solid triangles represent the Monte Carlo results (Ref. 24). The solid and dashed curves are calculated from the present DFT and nonlinear PB equations, respectively.

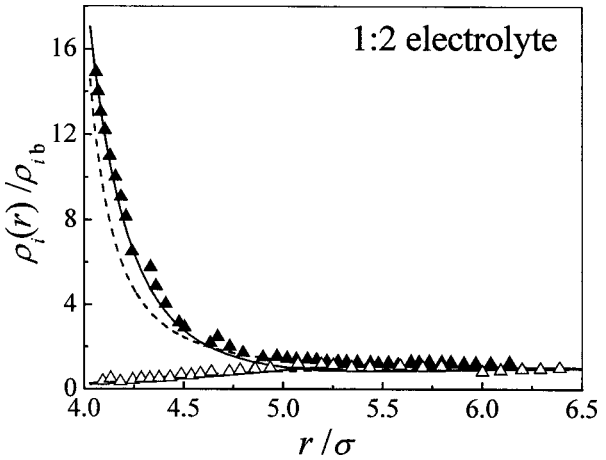

FIG. 3. Density profiles of counterions and coions around a charged spherical macroparticle of radius $R=1.5$ nm and surface charge density $Q=0.204$ C/m^2 in a 1:2 electrolyte at the bulk concentration $C=0.5$ mol/L. The symbols and curves have the same meaning as those in Fig. 1.

ion has a large size (e.g., $R=10.0$ nm). In the former case, the reduced ionic density profiles become identical to the radial distribution functions for the corresponding bulk electrolyte solution. In the latter case, there should be little difference between the spherical EDL and planar EDL. In both cases, our DFT results are in excellent agreement with the MC data,[7,57] showing that our DFT equations and the numerical method are reliable.

In Fig. 1, we plot the density profiles of coions and counterions around a charged spherical macroparticle of radius $R=1.5$ nm and surface charge density $Q=0.102$ C/m^2 dispersed in a 1:1 electrolyte at 1 mol/L. As expected, there is a significant accumulation of counterions near the charged macroparticle, accompanied by a depletion of coions in the same region. The density profiles of coion and counterion predicted from the DFT are very close to those from MC simulations.[24]

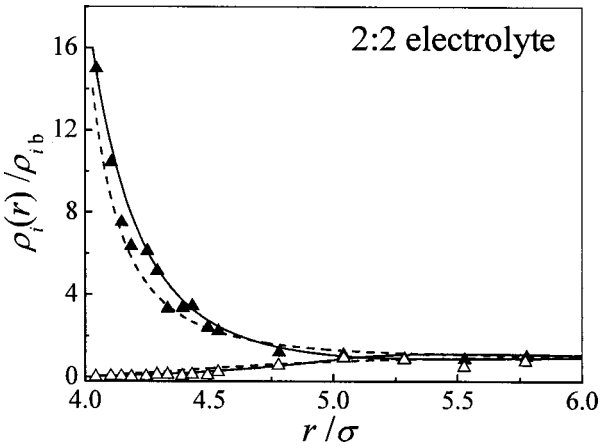

FIG. 2. Density profiles of counterions and coions around a charged spherical macroparticle of radius $R=1.5$ nm and charge density $Q=0.204$ C/m^2 in a 2:2 electrolyte solution at $C=0.5$ mol/L. The symbols and curves have same meaning as those in Fig. 1.

Figures 2 and 3 depict the density profiles of coions and counterions as a function of the radial distance from the center of a charged macroparticle immersed in 2:2 and 1:2 electrolyte solutions, respectively. In both cases, the counterions are divalent and the salt concentration is 0.5 mol/L. Both Figs. 2 and 3 show that in comparison with the MC data,[24,25] DFT is more accurate than the nonlinear PB theory, especially for the density profiles of counterions near the contact.

The nonlinear PB theory predicts only monotonic variations for the density profiles of both coions and counterions. However, the MC results of Torrie and Valleau,[7] Caillol and Levesque,[11] and Lamperski and Bhuiyan[58] for the structures of planar EDLs exhibit interesting layering effects when the surface charge densities are sufficiently high. Our DFT calculations as presented in Fig. 4 show that these layering effects also occur in spherical geometry. For 1:1 and 2:1 electrolytes around a hard spherical macroparticle with radius $R=1.5$ nm, the ionic reduced density profiles are monotonic in the case of surface charge densities $Q=0.102$ and 0.306 C/m^2. In contrast, at a surface charge density $Q=0.816$ C/m^2, a second layer of counterions is clearly formed for both 1:1 and 2:1 electrolytes. The layering effects are due to the interplay of the increased electrostatic attraction from the spherical macroparticle, the interionic correlations, and the hard-core exclusion by the macroparticle and small ions. The high surface charge densities lead to a substantial buildup of counterions next to the macroparticle surface. However, steric effects and interionic correlations preclude distant counterions from drifting too close to the macroparticle. These counterions then pack themselves into a second layer at next nearest optimum distance (around 1.5σ) from the macroparticle surface.[58,59] In addition, the increased surface charge density on the spherical macroparticle also causes an excessive accumulation of counterions near the macroparticle, accompanied by an excessive depletion of coions.

The effect of variation of the macroparticle radius on counterion layering can be seen in Fig. 5, where the surface charge density of the spherical macroparticle is 0.816 C/m^2.

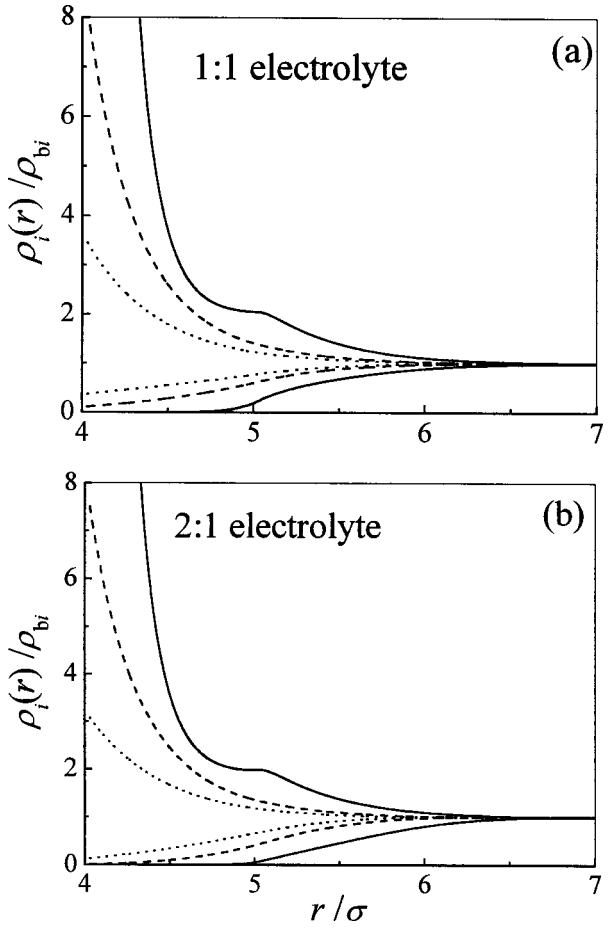

FIG. 4. Ionic density profiles from DFT for (a) 1:1 and (b) 2:1 electrolytes around a spherical macroparticle with radius $R=1.5$ nm and various surface charge densities. The bulk electrolyte concentrations are 1.0 and 0.5 mol/L for (a) and (b), respectively. The dotted, dashed, and solid curves are for $Q=0.102$, 0.306, and 0.816 C/m^2, respectively.

The height of the first and second layer peaks increases as the macroparticle radius increases. With regard to the first peak, this effect can be well explained even by the PB theory. Figure 5 shows that the second counterion layer peak disappears at the macroparticle radius $R=0.5$ nm. The predictions of the layering effects from the present DFT for high surface charge densities agree qualitatively with MC simulations for the planar EDL. In contrast, since the excluded volume is neglected, the nonlinear PB theory is unable to predict the layering effects. It should be pointed out that for a typical charged colloidal particle, the surface charge density is not larger than 0.3 C/m^2. Therefore, generally there is no second-layer formation around a realistic colloidal particle.

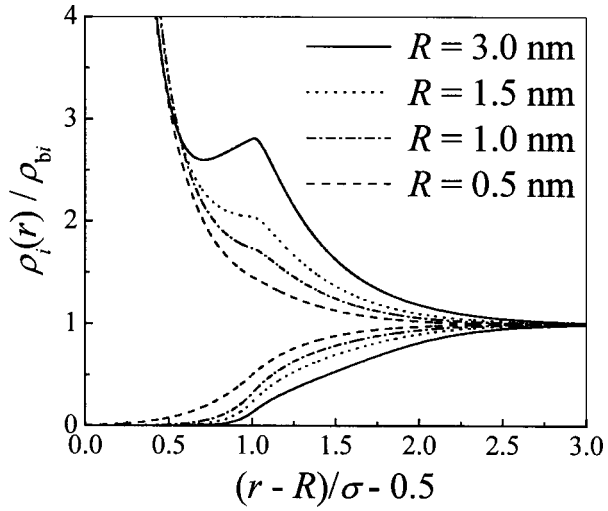

FIG. 5. Ionic density profiles from DFT for 1.0 mol/L 1:1 electrolyte around spherical macroparticles with surface charge density $Q=0.816$ C/m^2 and various radii.

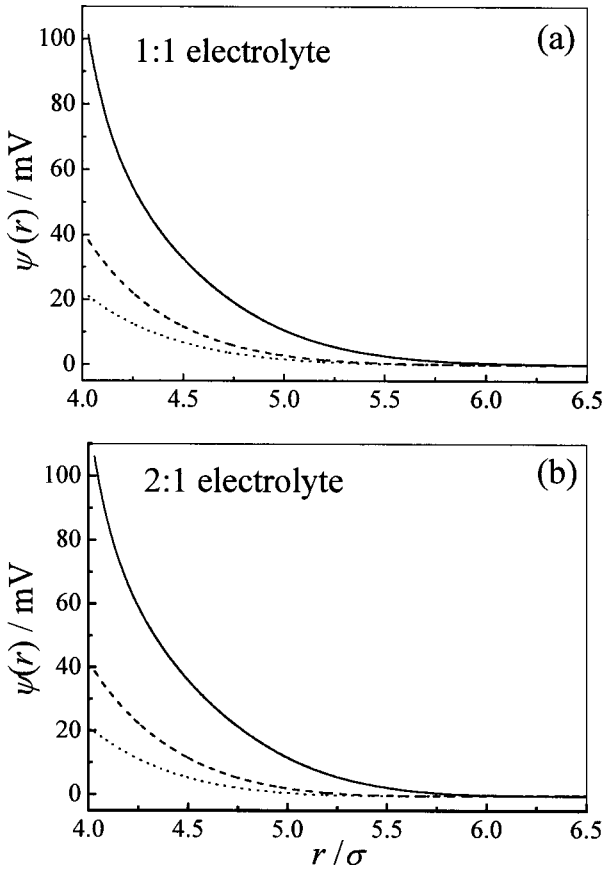

FIG. 6. Mean electrostatic potentials from DFT for (a) 1:1 and (b) 2:1 electrolytes around a spherical macroparticle with the radius $R=1.5$ nm and various surface charge densities. The bulk electrolyte concentrations are 1.0 and 0.5 mol\L for (a) and (b), respectively. The dotted, dashed, and solid curves correspond to $Q=0.102$, 0.306, and 0.816 C/m^2, respectively.

Figures 6(a) and 6(b) show the mean electrostatic potential profiles corresponding to the system shown in Fig. 4 for surface charge densities at $Q=0.102$, 0.306, and 0.816 C/m^2. In both cases, the DFT predicts a shallow minimum in the mean electrostatic potential. The similarity between Figs. 6(a) and 6(b) implies that the coions have little effect on the mean electrostatic potential. At a fixed electrolyte concentration, both the strength and range of the mean electrostatic potential increase with surface charge density, leading the diffuse layer to fall off gradually and extend quite a few ionic diameters into the solution. From Figs. 4 and 6 one can see that the properties of a spherical electric double layer are mainly determined by the counterions.

B. Zeta potential

The zeta potential ζ is defined as the mean electrostatic potential $\psi(r)$ at the closest separation between a small ion

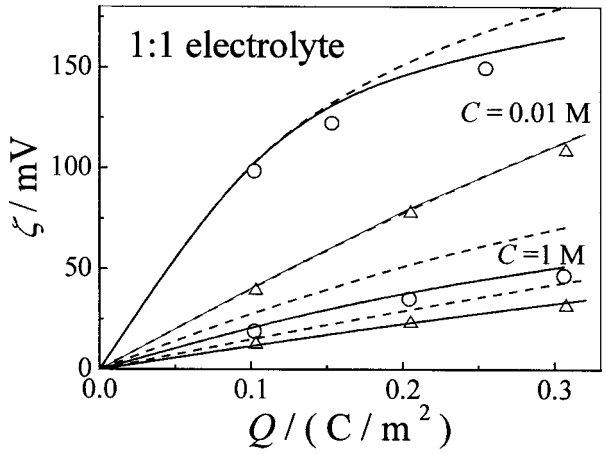

FIG. 7. Zeta potentials for a 1:1 electrolyte as a function of surface charge density of macroparticles with radius $R=1.5$ nm and $R=0.5$ nm. The open circles and open triangles represent the Monte Carlo simulation results (Refs. 24 and 25) for $R=1.5$ nm and $R=0.5$ nm, respectively. The dotted and solid curves represent the results of the PB and DFT, respectively. The HNC/MSA theory gives almost same results as the DFT in this case.

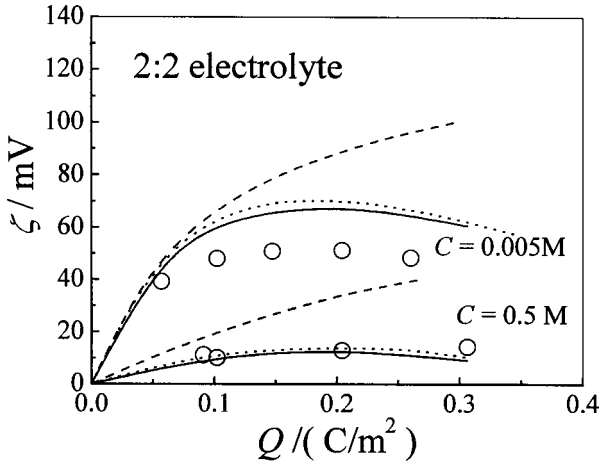

FIG. 8. Zeta potentials for a 2:2 electrolyte as a function of surface charge density of macroparticle with radius $R=1.5$ nm. The open circles represent the Monte Carlo simulation results (Refs. 24 and 25); the dotted, dashed, and solid curves represent the results of the HNC/MSA, PB, and DFT, respectively.

and the charged macroparticle—i.e., $\zeta=\psi(R+\sigma/2)$. In terms of the ionic density distributions, the ζ potential can be calculated from

$$\zeta=\frac{4\pi e}{\varepsilon}\int_{R+\sigma/2}^{\infty}dr\sum_i \rho_i(r)z_i\left[r-\frac{r^2}{R+\sigma/2}\right]. \tag{31}$$

In Figs. 7–9, we plot the ζ potentials of a macroparticle as a function of the surface charge density in 1:1, 2:2, and 2:1 electrolyte solutions, respectively. The concentrations of the electrolytes are 0.01 and 1 mol/L for 1:1 electrolytes and 0.005 and 0.5 mol/L for 2:2 and 2:1 electrolytes. In these figures, the radius of the macroparticle is fixed at $R=1.5$ nm or $R=0.5$ nm. Also plotted in these figures are the results from MC simulations, from the HNC/MSA integral equation, and from the nonlinear PB theory.[24,25] For the monovalent counterions at low concentrations (see Fig. 7), there is good agreement among HNC/MSA, nonlinear PB theory, the present DFT, and the MC simulation. In this case, the HNC/MSA integral equation gives essentially the same results as the present DFT. For the divalent counterions and/or at high electrolyte concentration, both HNC/MSA and DFT agree well with simulation results, whereas the nonlinear PB theory gives too large an absolute value of the ζ potential and fails to capture the maximum (or minimum) of the ζ potential as a function of the surface charge density (see Figs. 8 and 9). For divalent counterions, the results from the present DFT are slightly better than those from the HNC/MSA. Overall, the ζ potentials calculated from the DFT and HNC/MSA are in very good agreement with simulation results,[24,25] whereas the nonlinear PB theory overestimates the absolute values of the ζ potential. The similar behavior of the DFT and HNC/MSA can be explained by the fact that both theories are based on quadratic expansions and both use the same direct correlation functions for the bulk electrolyte solution from MSA.

From Figs. 8 and 9 one can see that both DFT and HNC/MSA predict a maximum (or a minimum) in the curves of the ζ potential as a function of surface charge density and this maximum (or minimum) is more pronounced in solutions of lower ionic concentration. The maximum (or minimum) in the ζ potential for the divalent counterion systems gives the interesting possibility that the diffuse layer differential capacitance can become infinite before becoming negative.[14] The strength of the ζ potential declines as the ionic concentration increases. These observations are consistent with that reported by Haydon[60] for the electrophoretic mobility of hydrocarbon droplets immersed in a NaCl solution.

In Figs. 10 and 11, ζ potential is plotted as a function of the inverse of macroparticle radius for the monovalent and divalent counterions, respectively. Here the macroparticle surface charge density is $Q=0.204\,\mathrm{C/m^2}$ and the electrolyte concentrations are 0.01 and 1 mol/L for 1:1 electrolyte and 0.005 and 0.5 mol/L for 1:2, 2:1, and 2:2 electrolyte solutions. As in Figs. 7–9, the nonlinear PB theory overestimates the ζ potential except at small values of the macroparticle

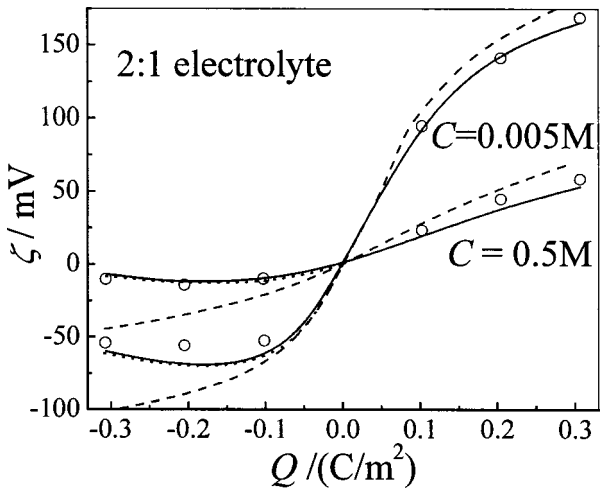

FIG. 9. Zeta potentials for a 2:1 electrolyte as a function of surface charge density of macroparticle with radius $R=1.5$ nm. The symbols and curves have the same meaning as those in Fig. 8.

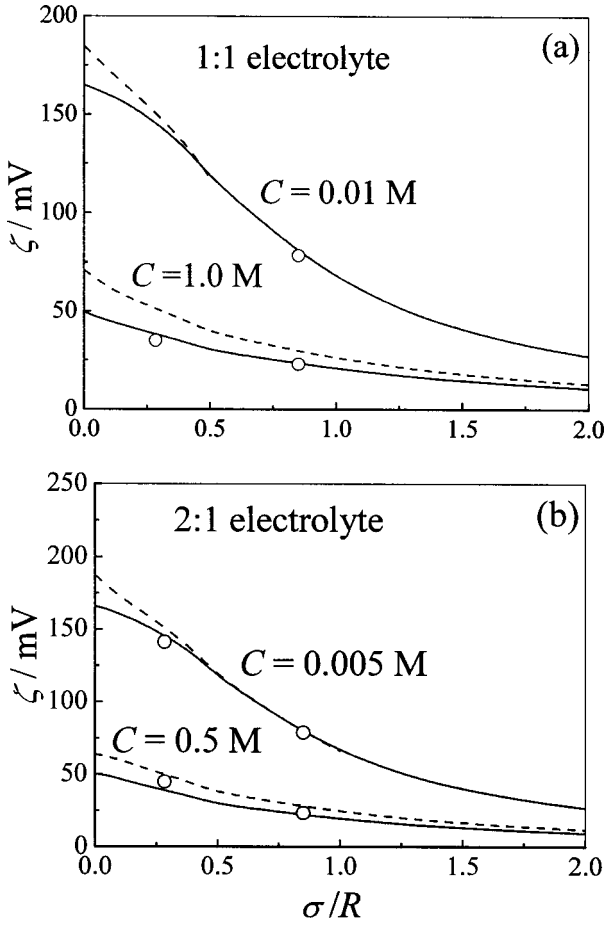

FIG. 10. Zeta potentials for (a) 1:1 and (b) 2:1 electrolytes as a function of the inverse of the macroparticle radius at the surface charged density $Q = 0.204\ \mathrm{C/m^2}$. In both cases the counterions are monovalent. The open circles represent the Monte Carlo simulation results (Refs. 24 and 25); the dashed and solid curves represent the results of PB and DFT, respectively.

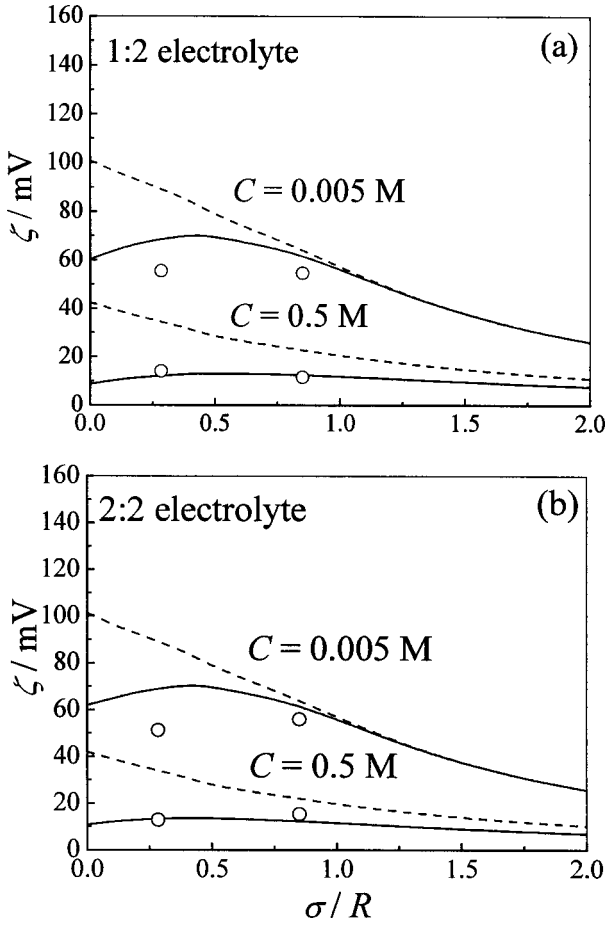

FIG. 11. Zeta potentials for (a) 1:2 and (b) 2:2 electrolytes as a function of the inverse of the macroparticle radius at the surface charged density $Q = 0.204\ \mathrm{C/m^2}$. In both cases the counterions are divalent. The open circles represent the Monte Carlo simulation results (Refs. 24 and 25). The dashed and solid curves represent the results of PB and DFT, respectively.

radius and low electrolyte concentrations. In all cases, the results from the present DFT are in good agreement with the MC data.[24,25] It is shown in Fig. 10 that for macroions dispersed in a solution containing only monovalent counterions, the ζ potential declines as the radius of the macroparticle falls while the surface charge density remains constant. The trend becomes more significant in dilute electrolyte solutions.

Figure 11 shows that the nonlinear PB theory is qualitatively different from the results from the present DFT and MC simulations[24,25] for the divalent counterions at large values of the macroparticle radius. According to the present DFT, there is a maximum in the curves of the ζ potential as a function of the inverse of the macroparticle radius for the divalent counterions. The nonlinear PB theory is unable to reproduce this maximum and predicts a monotonic increase of the ζ potential with an increase of the macroparticle radius for the divalent counterions.

C. Charge inversion

To characterize the oscillating behavior of charge density profiles, we define the integrated charge distribution functions $P(r)$:

$$P(r) = Z + \int_0^r \sum_i 4\pi z_i \rho_i(r') r'^2 dr'. \tag{32}$$

The integrated charge distribution function $P(r)$ represents the overall charge of the macroion and its surrounding ionic clouds within radius r. It can be easily calculated once we have the density profiles for the counterions and coions from DFT.

In Fig. 12 the present DFT results for the integrated charge distribution function $P(r)$ around a macroion are compared to the canonical ensemble (NVT) MC simulation results of Terao and Nakayama[46] for 2:2 electrolyte solution at an average concentration $C_{\mathrm{av}} = 1.25$ mol/L and temperature $T = 300$ K (the corresponding dielectric constant of water is $\varepsilon = 78$). In the NVT MC simulation of Terao and Nakayama,[46] the macroion with radius $R = 1.0$ nm and charge $Z = -20$ is placed in the center of the cubic simulation box with side length $L = 10.0$ nm. In addition to Z monovalent counterions, the systems contains additional ions from 2:2 electrolytes, where the average concentration of electrolytes in the box is 1.25 mol/L and the radius of all small ions is 0.4 nm. From Fig. 12 one can see that the predicted results from the present DFT are in good agreement with the MC simu-

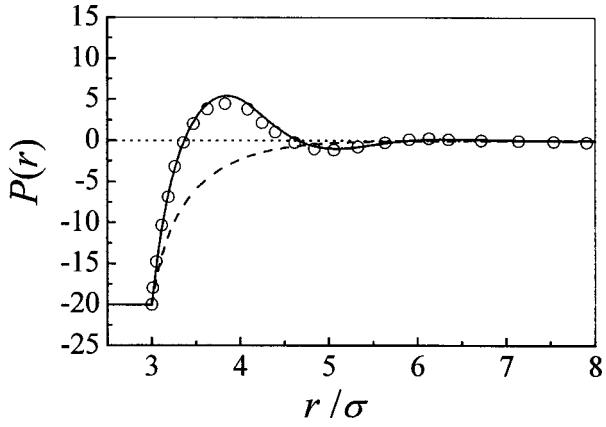

FIG. 12. Comparison between the predicted and *NVT* MC simulation results for the integrated charge distribution function around a macroion with radius $R=1.0$ nm and surface charge $Z=-20$ at $T=300$ K. There are Z monovalent counterions in the cubic simulation box and the average concentration for 2:2 electrolyte solution in the box is 1.25 mol/L. The diameter of small ions is $\sigma=0.4$ nm. The symbols represent the MC results. The dashed and solid curves represent the results of the PB and DFT, respectively.

lation data,[46] showing that the present DFT can be used to study the interesting charge inversion phenomena.

Using the DFT developed in this work, we calculated the integrated charge distribution functions around a spherical macroparticle of radius $R=1.5$ nm and a surface charge density $Q=-0.102\,\mathrm{C/m^2}$ (corresponding to surface charge number $Z=-18$) for 1:1, 2:1, and 2:2 electrolytes. The results are shown in Figs. 13(a)–13(c), respectively. At low electrolyte concentration ($C=0.05$ mol/L), Fig. 13 shows that $P(r)$ approaches zero monotonically as $r\to\infty$, indicating that the charged spherical macroparticle is fully screened at a distance much larger than the screen length. As the electrolyte concentration increases ($C=1.0$ mol/L), $P(r)$ for 2:1 and 2:2 electrolytes becomes positive at certain ranges of r, showing a charge inversion. This is because at larger concentrations of divalent counterions, the charged spherical macroparticles in the aqueous solution strongly bind so many oppositely charged small ions that the sign of the net macroparticle charge becomes inverted. The overscreening phenomenon may also be responsible for the attraction between like-charged colloidal particles.[47,49] At higher electrolyte concentrations, charge inversion occurs in all three types of electrolytes. To our knowledge, previous studies[46,61] did not find the charge inversion with monovalent counterions (at ambient conditions). Figure 13 shows that the charge inversion with the monovalent counterions is much weaker than that with the divalent counterions. In Figs. 13(b) and 13(c), the maximum of $P(r)$ is closer to the surface of macroparticles as the electrolyte concentration increases.

In Fig. 14 we plotted the reduced integrated charge distribution functions $P^*(r)=P(r)/|Z|$ for a charged spherical macroparticle of radius $R=1.5$ nm dispersed in a 2:2 electrolyte solution. Various surface charge densities are considered. The concentration of 2:2 electrolytes is fixed at $C=0.25$ mol/L. The charge inversion phenomenon is indeed observed, but only at sufficiently high surface charge density. The present DFT correctly predicts the occurrence of charge

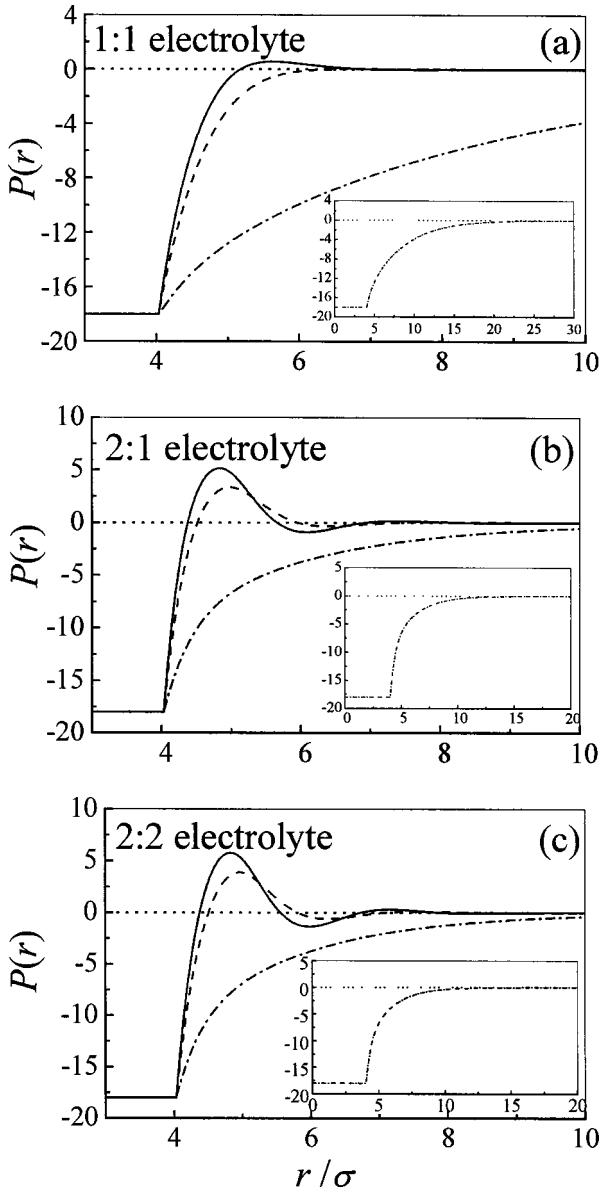

FIG. 13. Integrated charge distribution functions around a charged spherical macroparticle of radius $R=1.5$ nm and surface charge number $Z=-18$ calculated from DFT in (a) 1:1, (b) 2:1, and (c) 2:2 electrolyte solutions. The dash-dotted, dashed, and solid curves correspond to concentrations $C=0.05$, 1.0, and 1.5 mol/L, respectively. The insets give the full curves of charge distribution functions at concentration $C=0.05$ mol/L.

inversion at high electrolyte concentrations and/or high surface charge densities. The charge inversion phenomena predicted from the present DFT are consistent with the recent molecular dynamics simulation results given by Messina *et al.*[32] Our calculations suggest that, as proposed by Deserno *et al.*[20] and Messina *et al.*,[32] the local ion-size correlations are responsible for the charge inversion phenonmena. The charge inversion becomes more significant with an increase of the excluded-volume effects in the system—i.e., at higher ionic size and/or concentrations. As shown in Fig. 13(a), charge inversion occurs even for macroions surrounded by monovalent counterions.

IV. CONCLUDING REMARKS

A density-functional theory has been proposed for the density distributions of small ions around a charged spherical

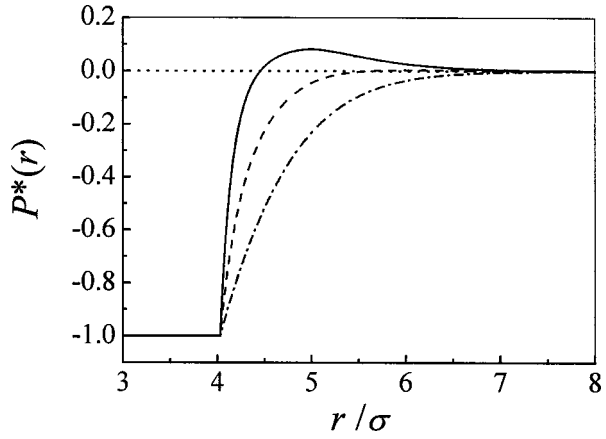

FIG. 14. Reduced integrated charge distribution function $P^*(r)$ for 2:2 electrolyte around a macroparticle of radius $R=1.5$ nm and various surface charge densities at bulk concentration $C=0.25$ mol/L. The dash-dotted, dashed, and solid curves correspond to surface charge density $Q=-0.051$, -0.204, and -0.295 C/m^2, respectively.

macroparticle. The theory is partially perturbative since the hard-sphere contribution to the free-energy functional is evaluated from the improved fundamental measure theory and the electrical contribution is approximated by a quadratic expansion with respect to the corresponding bulk fluid. Extensive comparison with Monte Carlo simulations indicates that the present DFT provides accurate ionic density distributions for a charged spherical macroparticle immersed in 1:1, 1:2, 2:1, and 2:2 electrolyte solutions. The present DFT successfully predicts the properties of counterion layering at high surface charge density in a spherical EDL. It is concluded from the present DFT that an increase of the surface charge density or the radius of the spherical particle enhances the tendency for the formation of the second counterion layer.

The results from the present DFT are also compared to those from the nonlinear Poisson–Boltzmann theory and the hypernetted-chain–mean-spherical approximation integral equation theory. All these theories are in good agreement with Monte Carlo simulation data for monovalent counterions at low concentration. For divalent counterions and/or high concentrations, however, the results from the present DFT and HNC/MSA theory are better than that from the nonlinear PB equation. For divalent counterions and/or high concentration, the ζ potential from the PB theory is qualitatively different from that obtained through the present DFT and HNC/MSA theory. The present DFT and HNC/MSA theory predict a maximum (or a minimum) ζ potential as a function of the surface charge density or macroparticle radius, while the nonlinear PB theory is unable to predict this maximum (or minimum). The present DFT gives a slightly better ζ potential than the HNC/MSA for divalent counterions, but for monovalent counterions, the two theories give almost identical results. The similarity is due to the fact that both theories use the direct correlation function for bulk fluid from the MSA. In addition, the qualitative behavior of the ζ potentials from the present DFT are consistent with observations from eletrophoretic mobility experiments.[60,62]

We have also investigated the integrated charge distribution function around a charged spherical macroparticle. The charge oscillation and charge inversion phenomena have been found for high electrolyte concentration and/or large surface charge density. Interestingly, the charge inversion can occur even for monovalent counterions at high ionic size and/or concentration, which is different from the general belief.[46,61] From the DFT calculations we conclude that the excluded volume plays a crucial role in the charge inversion. The nonlinear PB theory is unable to predict charge inversion phenomena because it ignores ionic size. In the PB theory, charged colloidal particles are surrounded by oppositely charged counterions and the overlap of the counterion atmosphere produces a purely repulsive interaction between like-charged colloidal particles. Our results from the DFT indicate that the above picture does not hold when the surface charge density on the colloidal particles or the electrolyte concentration is sufficiently high.

Because the improved fundamental measure theory is directly applicable to mixtures and the analytical expressions for the direct correlation functions of bulk mixed electrolyte solutions are available in the literature,[63] extension of the present DFT to study the distributions of real mixed electrolytes around a realistic charged colloidal particle is relatively straightforward. To further improve the quantitative performance of the present DFT, one may treat the bulk electrolyte by means of more elaborate theories for the direct correlation functions—for instance, the generalized mean spherical approximation,[44] which is thermodynamically self-consistent and still analytical. It is also possible to include the solvent (water) as a third component in the solution if the interactions are pairwise decomposable and a theory for the bulk uniform fluid is available.[43] With these improvements, the present DFT will be potentially useful to investigate the ζ potential and eletrophoretic mobility of colloidal particles in solution including proteins in aqueous electrolyte solutions.

ACKNOWLEDGMENTS

This work is sponsored in part by the University of California Research and Development Program (Grant No. 69757), by Lawrence Livermore National Laboratory (Grant No. MSI-04-005), and by the National Science Foundation (Grant No. CTS-0340948). Y.Y.-X. and G.G.-H. gratefully acknowledge financial support from the National Natural Science Foundation of China (Grant No. 20176020).

[1] P. C. Hiemenz and R. Rajagopalan, *Principles of Colloid and Surface Chemistry* (Dekker, New York, 1997); A. W. Adamson and A. P. Gast, *Physical Chemistry of Surfaces* (Wiley, New York, 1997); W. B. Russel, D. A. Saville, and W. R. Schowalter, *Colloidal Dispersions* (Cambridge University Press, Cambridge, England, 1989).
[2] R. J. Hunter, *Foundations of Colloid Science* (Oxford University Press, New York, 1985).
[3] E. Gonzalez-Tovar and M. Lozada-Cassou, J. Phys. Chem. **93**, 3761 (1989).
[4] K.-L. Yang, S. Y. Yiacoumi, and C. Tsouris, J. Chem. Phys. **117**, 8499 (2002).
[5] E. Gonzalez-Tovar, M. Lozada-Cassou, and D. Henderson, J. Chem. Phys. **83**, 361 (1985).
[6] M. Lozada-Cassou, E. Gonzalez-Tovar, and W. Olivares, Phys. Rev. E **60**, R17 (1999).
[7] G. M. Torrie and J. P. Valleau, J. Chem. Phys. **73**, 5807 (1980); J. Phys. Chem. **86**, 3251 (1982).

[8] M. Lozada-Cassou, R. Saavedra-Barrera, and D. Henderson, J. Chem. Phys. **77**, 5150 (1982).
[9] L. Mier-y-Teran, E. Diaz-Herrera, M. Lozada-Cassou, and D. Henderson, J. Phys. Chem. **92**, 6408 (1988).
[10] L. Mier-y-Teran, S. H. Suh, H. S. White, and H. T. Davis, J. Chem. Phys. **92**, 5087 (1990); C. N. Patra and S. K. Ghosh, *ibid.* **100**, 5219 (1994); **101**, 4143 (1994).
[11] J. M. Caillol and D. Levesque, J. Chem. Phys. **94**, 597 (1991).
[12] E. Kierlik and M. L. Rosinberg, Phys. Rev. A **44**, 5025 (1991).
[13] H. Greberg, R. Kjellander, and T. Akesson, Mol. Phys. **92**, 35 (1997).
[14] D. Boda, W. R. Fawcett, D. Henderson, and S. Sokolowski, J. Chem. Phys. **116**, 7170 (2002).
[15] D. Boda, D. Henderson, L. Mier-y-Teran, and S. Sokolowski, J. Phys.: Condens. Matter **14**, 11945 (2002).
[16] C. N. Patra and S. K. Ghosh, J. Chem. Phys. **117**, 8938 (2002).
[17] P. S. Crozier, R. L. Rowley, and D. Henderson, J. Chem. Phys. **114**, 7513 (2001).
[18] S. L. Carnie and G. M. Torrie, Adv. Chem. Phys. **56**, 141 (1984).
[19] C. N. Patra and A. Yethiraj, J. Phys. Chem. B **103**, 6080 (1999).
[20] M. Deserno, F. Jimenez-Angeles, C. Holm, and M. Lozada-Cassou, J. Phys. Chem. B **105**, 10983 (2001).
[21] M. Lozada-Cassou, J. Phys. Chem. **87**, 3729 (1983); R. Backet and P. J. Rossky, *ibid.* **88**, 2660 (1984); B. Hribar, V. Vlachy, L. B. Bhuiyan, and C. W. Outhwaite, J. Phys. Chem. B **104**, 11522 (2000).
[22] C. N. Patra and A. Yethiraj, Biophys. J. **78**, 699 (2000).
[23] C. W. Outhwaite and L. B. Bhuiyan, Mol. Phys. **74**, 367 (1991).
[24] L. Degreve, M. Lozada-Cassou, E. Sanchez, and E. Gonzalez-Tovar, J. Chem. Phys. **98**, 8905 (1993).
[25] L. Degreve and M. Lozada-Cassou, Mol. Phys. **86**, 759 (1995).
[26] A. L. Loeb, J. T. G. Overbeek, and P. H. Wiersema, *The Electric Double Layer around a Spherical Colloid Particle* (MIT Press, Cambridge, MA, 1961).
[27] G. Rickayzen, J. Chem. Phys. **111**, 1109 (1999); A. I. Bulavchenko, A. F. Batishchev, E. K. Batishcheva, and V. G. Torgov, J. Phys. Chem. B **106**, 6381 (2002).
[28] W. R. Bowen and F. Jenner, Chem. Eng. Sci. **50**, 1707 (1995); W. R. Bowen and P. M. Williams, J. Colloid Interface Sci. **184**, 241 (1996); S. N. Petris, D. Y. C. Chan, and P. Linse, J. Chem. Phys. **118**, 5248 (2003).
[29] E. Wigner and F. Seitz, Phys. Rev. **43**, 804 (1933); R. J. F. L. de Carvalho, E. Trizac, and J. P. Hansen, Phys. Rev. E **61**, 1634 (2000); E. Trizac and J. P. Hansen, *ibid.* **56**, 3137 (1997); J. Phys.: Condens. Matter **9**, 2683 (1997).
[30] J. P. Hansen and H. Lowen, Annu. Rev. Phys. Chem. **51**, 209 (2000).
[31] Y. Levin, Rep. Prog. Phys. **65**, 1577 (2002).
[32] R. Messina, E. Gonzalez-Tovar, M. Lozada-Cassou, and C. Holm, Europhys. Lett. **60**, 383 (2002).
[33] T. T. Nguyen and B. I. Shklovskii, Phys. Rev. E **64**, 041407 (2001).
[34] R. Messina, C. Holm, and K. Kremer, Phys. Rev. E **64**, 021405 (2001).
[35] U. P. Strauss, N. L. Gershfeld, and H. Spiera, J. Am. Chem. Soc. **76**, 5909 (1954).
[36] W. van Megen and I. Snook, J. Chem. Phys. **73**, 4656 (1980).
[37] G. N. Patey, J. Chem. Phys. **72**, 5763 (1980); D. Bratko, H. L. Friedman, and E. C. Zhong, *ibid.* **85**, 377 (1986).
[38] L. B. Bhuiyan and C. W. Outhwaite, J. Chem. Phys. **116**, 2650 (2002); L. B. Bhuiyan, V. Vlachy, and C. W. Outhwaite, Int. Rev. Phys. Chem. **21**, 1 (2002); S. Lamperski and C. W. Outhwaite, Langmuir **18**, 3423 (2002).
[39] M. Lozada-Cassou and E. Gonzalez-Tovar, J. Colloid Interface Sci. **239**, 285 (2001).
[40] A. Martin-Molina, M. Quesada-Perez, F. Galisteo-Gonzalez, and R. Hidalgo-Alvarez, J. Phys. Chem. **106**, 6881 (2002).
[41] Z. X. Tang, L. Mier-y-Teran, H. T. Davis, L. E. Scriven, and H. S. White, Mol. Phys. **71**, 369 (1990).
[42] Z. X. Tang, L. E. Scriven, and H. T. Davis, J. Chem. Phys. **97**, 494 (1992); **97**, 9258 (1992); **100**, 4527 (1994); D. Goulding and J. P. Hansen, Europhys. Lett. **46**, 407 (1999).
[43] T. Biben, J. P. Hansen, and Y. Rosenfeld, Phys. Rev. E **57**, R3727 (1998).
[44] G. Stell and S. F. Sun, J. Chem. Phys. **63**, 5333 (1975).
[45] R. Messina, C. Holm, and K. Kremer, Comput. Phys. Commun. **147**, 282 (2002); B. I. Shklovskii, Phys. Rev. Lett. **82**, 3268 (1999).
[46] T. Terao and T. Nakayama, Phys. Rev. E **63**, 041401 (2001).
[47] T. T. Nguyen, A. Y. Grosberg, and B. I. Shklovskii, J. Chem. Phys. **113**, 1110 (2000).
[48] M. Tanaka and A. Y. Grosberg, J. Chem. Phys. **115**, 567 (2001).
[49] H. Greberg and R. Kjellander, J. Chem. Phys. **108**, 2940 (1998); R. Messina, C. Holm, and K. Kremer, Phys. Rev. Lett. **85**, 872 (2000).
[50] A. Y. Grosberg, T. T. Nguyen, and B. I. Shklovskii, Rev. Mod. Phys. **74**, 329 (2002).
[51] Y.-X. Yu and J. Z. Wu, J. Chem. Phys. **117**, 10156 (2002); **119**, 2288 (2003).
[52] R. Roth, R. Evans, A. Lang, and G. Kahl, J. Phys.: Condens. Matter **14**, 12063 (2002).
[53] Y. Rosenfeld, J. Chem. Phys. **93**, 4305 (1990); Phys. Rev. Lett. **63**, 980 (1989); J. Chem. Phys. **98**, 8126 (1993).
[54] T. Boublik, J. Chem. Phys. **53**, 471 (1970); G. A. Mansoori, N. F. Carnahan, K. E. Starling, and T. W. Leland, Jr., *ibid.* **54**, 1523 (1971).
[55] G. Zerah and J. P. Hansen, J. Chem. Phys. **84**, 2336 (1986).
[56] E. Waisman and J. L. Lebowitz, J. Chem. Phys. **56**, 3086 (1972); **56**, 3093 (1972).
[57] D. N. Card and J. P. Valleau, J. Chem. Phys. **52**, 6232 (1970).
[58] S. Lamperski and L. B. Bhuiyan, J. Electroanal. Chem. **540**, 79 (2003).
[59] P. Nielaba and F. Forstmann, Chem. Phys. Lett. **117**, 46 (1985).
[60] D. A. Haydon, Proc. R. Soc. London, Ser. A **258**, 319 (1960).
[61] B. Jonsson, H. Wennerstron, and B. Halle, J. Phys. Chem. **84**, 2179 (1980).
[62] H.-M. Lee, Y. W. Kim, and J. K. Baird, J. Cryst. Growth **232**, 294 (2001).
[63] K. Hiroike, Mol. Phys. **33**, 1195 (1977).